Experiments and modelling of electrospinning process

T.A. KOWALEWSKI*, S. BŁOŃSKI, and S. BARRAL

Institute of Fundamental Technological Research, Polish Academy of Sciences, 21 Świętokrzyska St., 00-049 Warszawa, Poland

Abstract. Very thin liquid jets can be obtained using electric field, whereas an electrically-driven bending instability occurs that enormously increases the jet path and effectively leads to its thinning by very large ratios, enabling the production of nanometre size fibres. This mechanism, although it was discovered almost one century ago, is not yet fully understood. In the following study, experimental data are collected, with the dual goal of characterizing the electro-spinning of different liquids and evaluating the pertinence of a theoretical model.

Key words: nanofibres, electrospinning, polymer fibres, electrified liquid jet.

1. Introduction

Nanotechnology has become in recent years a topic of great interest to scientists and engineers, and is now established as a prioritised research area in many countries. The reduction of the size to the nano-meter range brings an array of new possibilities in terms of material properties, in particular with respect to achievable surface to volume ratios. A variety of applications are being currently considered for nano-structural materials, including composites with reinforcing carbon nano-tubes, whiskers or nano-clay platelets, metal nanotubes (metallisation followed by polymer degradation), electrically conductive nano-fibres (polyaniline, coatings, nano-electronic machines), encapsulation of micro particles/compounds with drug action for burns treatment and wound healing/dressing, high performance/multifunctional filters (dust, bacteria, viruses) as well as applications in biomedicine with the use of biomaterial polymers (scaffold fabrication, protein fibres in arterial walls, coatings on prosthetic devices for implants).

The production of nano-scale dimension materials is not a trivial task. One of the simplest possibilities to reach small size is the mechanical elongation of a melt material and production of thin wires or fibres. This technique, well developed in the textile industry, has intrinsic physical limitations mainly related to hydrodynamic instabilities and mechanical constraints. Hence, two approaches have been recently developed to facilitate the production of nanofibres, namely electrospinning of nanofibres from polymer solutions or melts, and production of nanofibres by the so-called flash-spinning or melt-blown technique. The versatility of electrospinning makes it particularly interesting [1], as it has been already applied to more than 20 different polymer types including PA, PP, PE, PAN, PEO, Nylon-6, polyaniline and aramids [2–4].

The use of knowledge involving surface engineering at molecular and atomic level creates new perspectives for the production of multifunctional textile materials and nonwoven materials [5], with tailored (comfort, medical, technical) properties. Applications such as controlled wettability, adhesion of biological, organic deposits (washing and cleaning), chemi-

cal activity (coloration), barrier properties (gases, liquids, heat, magnetic field, harmful radiations, antibacterial), bioactivity, bio-compatibility, optical characteristics (photochromic, UV protection, sensors) are in sight. An interesting field is electronics where the use of electrospun fibres is being considered for the design of electronic circuits [6–8].

2. Electrospinning vs. classical spinning process

Formation of fibres by elongating slender liquid jets is a well established approach in textile industry. Typically, a molten polymer leaves an orifice and rapidly hardens due to heat or mass transfer to the environment or due to chemical reactions. The fibre is then "wound-up" downstream while large body forces exerted along the fibre stretch the jet.

Instability of the liquid column and mechanical fracture of the fibre are the main limitations of the process. In the absence of external forces, the resulting radius of the jet depends on the orifice diameter only. Due to surface tension and interfacial forces at the orifice it is impossible to directly generate very thin jets in the micrometer range, so that stretching appears as the only alternative to bypass this limit. For highly viscous, Newtonian fluids (water-glycerol solutions), gravitational stretching may lead to two orders of magnitude thinning of the jet (Fig. 1), [9]. However, due to the capillary instability and to aerodynamic forces, the length of liquid filaments obtained in such a way is limited to a few hundreds diameters only.

The stability problem of liquid jets dramatically changes for non-Newtonian fluids [10]. Formation of very long liquid filaments from polymers led to successful commercial applications to produce synthetic textiles. A polymer, usually melted, is fed into capillaries of a multifilament spinneret. The extruded filaments are drawn down to smaller diameters by action of a godet roll to winder [11]. A typical take-up velocity may reach hundreds of meters per second and extension ratio of a few hundred percent. Using classical spinning technique it is possible to obtain filaments of a few micrometers over an elongation distance of several meters. Further elongation becomes

---

practically very difficult to achieve. A distance between spinneret and winder needs to be extended to several kilometres to reach nano-size fibres. Even so, controlling filament stability over such a distance would not be practically achievable.
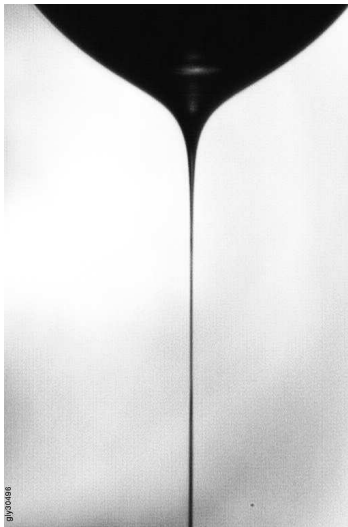

Fig. 1. Glycerol jet issued from a 0.2 mm nozzle and elongated gravitationally to a 5 μm thread (after Ref. 9)

Electrospinning occurs when the electric forces at the surface of a polymer solution or melt overcome the surface tension and cause an electrically charged jet to be ejected. The use of electrostatic forces may lead to new ways for farther elongation of material. It was already observed by Rayleigh [12] that a thin liquid jet issues from an electrically charged pendant droplet. This effect has been investigated in details by Taylor [13], who solved a stability problem for the surface shape of charged droplets that highlighted the existence of a critical angle for the droplet tip, called the "Taylor cone". Observations of liquid jetting from the droplet tip have been reported as indicators of electro-spraying, i.e. dispersion of the liquid to a mist of micro droplets. The droplets seemed to form a characteristic dispersion cone, distinctly visible with the naked eye or with a standard camera. High speed imaging gave evidence that the cone is actually an envelope of the bending loops of a spinning jet [14,15]. Indeed, the charged liquid jet is submitted to a spiralling motion when accelerated towards the collector. For solidifying polymers, the looping instability results in extreme elongation values. The axial tension of a fibre, provided by electrostatic forces, leads to elongation ratios of 10000 and more without breaking the thread [1]. The resulting nanofibre is often collected as an interconnected web of thin filaments (fibre mat) on the surface of a grounded target. The process, patented already in 1934 [16], is called electrospinning.

Various parameters, including the electric field intensity, the solution viscosity, the polymer relaxation time, the electric resistance, and the charge carried by liquid jet affect electrospinning, as indicated by parametric study performed by Theron et al. [2]. For dilute polymer solutions and Newtonian liquids, surface tension may also modify the fibre stability [2,17,18]. Gravity seems to be negligible and some re-

ports demonstrated successful electrospinning against gravitation [19]. Observations indicate that electrospinning is possible for non-Newtonian as well as for Newtonian fluids, but the range of optimal parameters for its initiation is yet difficult to predict.

Despite the simplicity of the electrospinning technology industrial applications of electrospinning are still relatively rare, mainly due to the unresolved problem of very low fibre throughput for existing devices [19]. Collection of experimental data and their confrontation with simple physical models appears as an effective approach towards the development of practical tools for controlling and optimising the electrospinning process. In the following, we present examples of electrospinning experiments performed in our laboratory and results of numerical simulations, based on a simplified physical description of the main phenomena involved.

3. Experimental

In the experiment a pendent droplet of the investigated polymer solution is supported by surface tension at the tip of a glass pipette. A thin silver wire is immersed in the pipette that applies a potential bias to the liquid. About 20 cm below the tip of pipette a copper grid plays the double role of collector and ground electrode. Due to the surface tension the droplet is initially in equilibrium with gravitational forces and prevents the solution to flow from the pipette. When the potential difference between the pipette and the collector is increased above about 5 kV, the electrical forces acting on charges induced in the liquid overcome the forces associated with surface tension. The electrically charged liquid jet emerges from a conical appendage that is created at the droplet surface. Since straight electrified liquid jets are unstable in the presence of electrical field, a bending instability develops shortly after the jet emerges from the tip. Some possible origins for the initial perturbation are non-uniformity of the electric field or local temperature fluctuation at the liquid surface. Once the bending appears, it generates a sequence of helical loops as a result of the interaction of repulsion forces between charges trapped in the jet and stabilizing forces of surface tension, viscoelasticity (if present) and applied electrical field. The diameter of the loops reaches several centimetres while their average downward velocity remains relatively low ($\sim$1 m/s). Hence, the elongation forces acting on the jet during few milliseconds of its flight into the collector result in enormous thinning of the jet diameter. Figure 2a shows electrified liquid jet recorded with standard video framing time (30 fps). The initial jet looks as though it splits into a bunch of secondary liquid treads, a process described as "splaying" by Doshi and Renecker [20]. High speed imaging using video camera with 4500 fps (Fig. 2b) reveals, however, a drastically different picture. The multijetting seen in the previous figure appears to be a mere optical illusion, created by the superposition of multiple light reflections from several loops. The jet emerging from the pipette preserves a continuous form, eventually forming a sequence of strongly bent loops.

Analysing single frames from the high speed camera, it is

possible to follow the evolution of the jet shape. However, only the initial thickness and primary thinning of the jet can be quantitatively evaluated using such images. The outcome of electrospinning becomes evident only after analysing under microscope the web-like structure collected on the ground electrode (Fig. 3a).

Characterisation of the electrospinning process is not a simple task, neither experimentally nor theoretically. The bending instability of an electrified jet is far from being a well controllable and reproducible phenomenon. The observed looping motion of the jet changes its amplitude and pitch in a stochastic way. This significantly differs from the well known buckling instability [21], typical for viscous jets interacting with a plane collector. Therefore the structure of collected nano-web is usually very irregular and special focusing techniques [22] are necessary to obtain a partially ordered material.
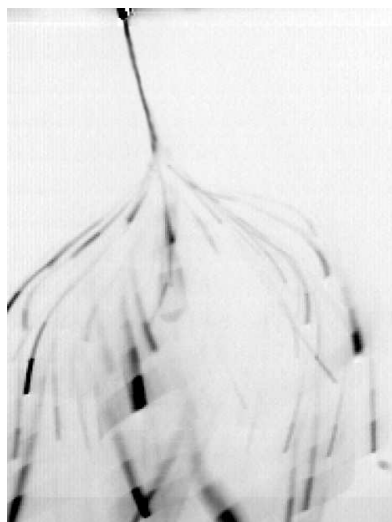

(a)
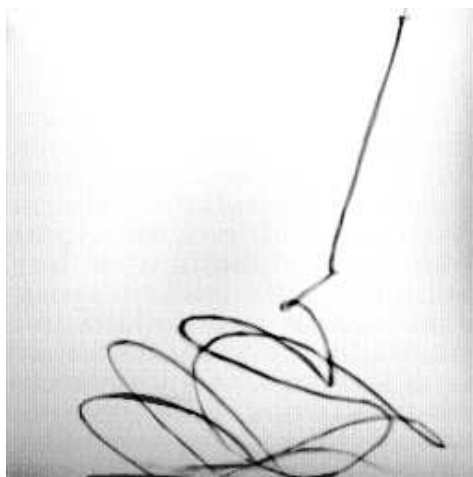
(b)

Fig. 2. Development of the bending instability for 0.1 mm jet of polyethylene-oxide water-alcohol solution. The measured average velocity of the jet is about 2 m/s and the electric potential 7.5 kV for a 20 cm height; image obtained with standard camera, exposure time 33 ms (a), high speed camera imaging, exposure time 0.1 ms. The image width corresponds to 40mm physical length (b)
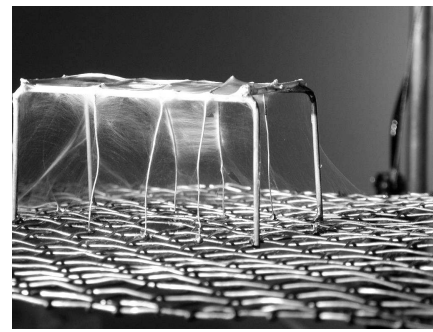
(a)
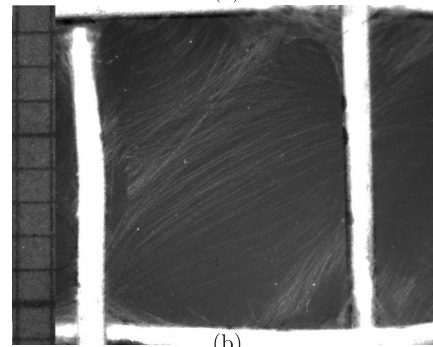
(b)
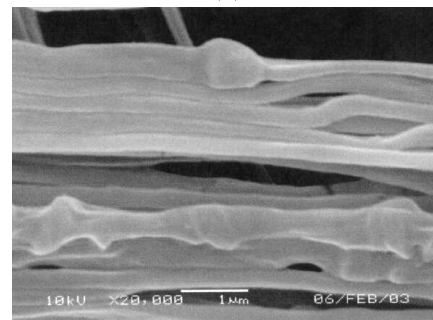
(c)

Fig. 3. Nanofibres of polyethylene-oxide: web like structure observed on the collector (a), sample from the collector under optical microscope, image width 15 mm (b), the same sample under electron microscope, image width 7 μm (c)

To reveal the main factors driving the electrospinning mechanisms two global characteristics have been evaluated from the experiment: the length of the straight part of the jet before bending instability occurs, and the initial angle of the looping envelope. The main factors affecting the process are the electrical potential and liquid properties. A simple approximation proposed by Reneker et al. [14] predicts a nearly linear increase of the straight segment with the applied voltage. According to this model the initial angle of the looping envelope strongly depends on evaporation and solidification rate for the polymer solutions. Nevertheless, the expected tendency is a decrease of the loop radius (and the envelope angle) with increasing electric potential. These general predictions are verified for three different polymer solutions. The most important parameter for a robust electrospinning process is the solution viscoelasticity. For comparison, the electrospinning of a Newtonian fluid, glycerol, is also characterized. The basic parameters of the fluids used are summarized in Table 1.

T.A. Kowalewski, S. Błoński, and S. Barral

Table 1

Main characteristics of four sets of electrospinning experiments

Material	Solvent	Kinematic viscosity* ν [mm²/s]	Concentration C_{wt} [%]	Φ [kV]	Comments on electrospinning
PEO – polyethyleneoxide (M = 4×10^5 g/mol)	40% ethanol – water solution	85–113	3–4	3–12	good and stable process for voltage up to 10 kV
DBC – dibutyrylchitin	ethanol	15	9	6–16	fairly good
PAN – polyacrylonitrile	DMF (dimethyl-formamide)	19	15	5–25	good
glycerol	water	150	88	20–30	difficult (no solidification)

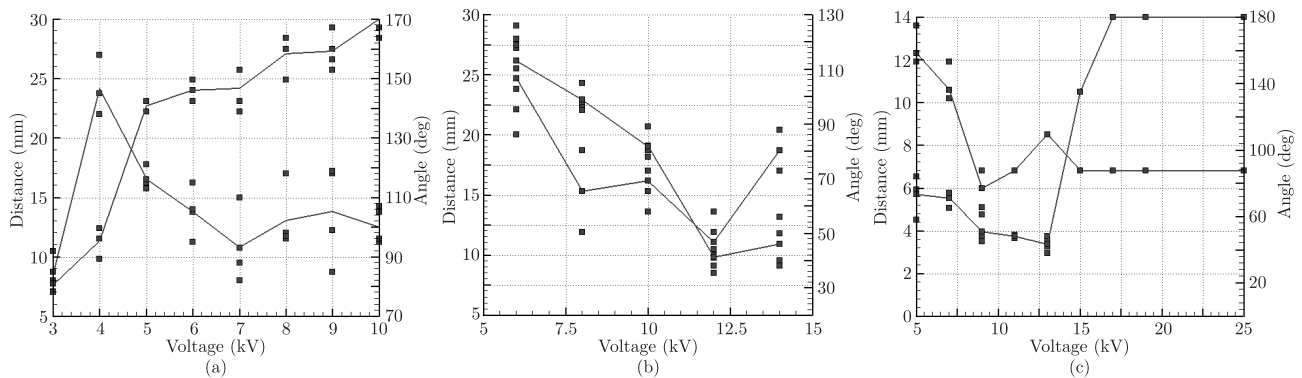* zero shear rate viscosity limit for non-Newtonian liquids given as reference

Fig. 4. Effect of the applied voltage on the length of the straight segment (left ordinate) and the spiral envelope angle (right ordinate) for three investigated polymer solutions: 4% PEO (a), 9% DBC (b), 15% PAN (c) (comp. Table 1)
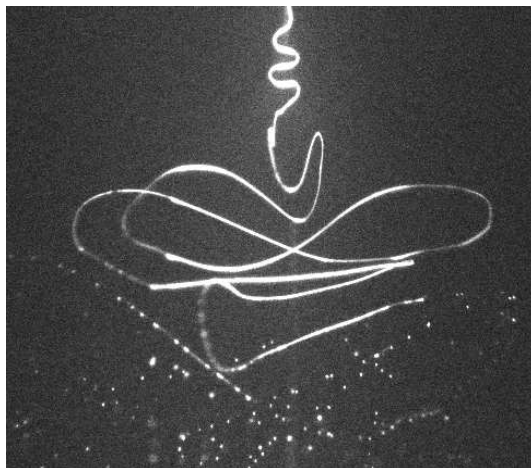

Fig. 5. Electrospinning of an 88% glycerol solution (comp. Table 1), actual image width: 65 mm

The experiments are performed at room temperature under normal atmospheric pressure. Bright field illumination using Fresnel lens and high speed CCD camera (Fastcam Roper Scientific) are used to capture movies of the spinning jet. The typical recording speed is 4500 fps (comp. Fig. 2b). A high resolution PIV camera (PCO) and double pulsed NdYag laser are used for measuring the velocity of the jet. For this purpose a very small amount of 50 nm fluorescent particles are added to the solution and their displacement recorded using laser light pulses of 5 ns duration. The system permits to record the motion of jet segments, to visualize the looping structure and to estimate the flow velocity in the upper segments of the jet. The pipette and grounded collector are closed in a 50 cm × 50 cm × 80 cm Plexiglas box to protect the electronic camera from electrostatic discharge and to avoid disturbances from ambient air motion.

A typical appearance of the electrically charged jet of PEO polymer solution is shown in Fig. 2b. The path of the jet formed at the tip of a pendant droplet is characterised by three distinct segments. The first one is a classical straight or slightly curved cylinder with typical length of several millimetres. Its length varies nearly linearly with the electrical potential applied and depends on the liquid properties. The second segment starts by a sudden bending instability of the straight cylinder, leading to the development of a conical spiral. The spiral height and diameter may reach several centimetres. The diameter of the upper part of the jet changes from 0.2 mm to about 50 µm for the first loop. The jet velocity in its upper parts, estimated using fluorescent particles, is relatively low. For the investigated PEO solution it is about 1 m/s at 3 kV and rises nearly linearly to 2.5 m/s at 10 kV. The growth rate of the spiral diameter depends on the electrical potential and fluid properties. After following several loops the conical shape be-

comes distorted. Large, irregular loops characterize the last jet segments, which are finally collected on the metal electrode. The diameter of the collected fibres can be as small as 50–100 nm, leading to a stretching factor of more than a thousand (Fig. 3b,c). Precise measurements of the jet geometry and velocity in its lower segments could not be performed. Microscopic close-up imaging is necessary for such measurements. However, a too close presence of the camera deforms the local electrostatic field attracting the jet, and in addition exposes the electronic to harmful corona discharges.

The onset of the electrospinning instability is strongly conditioned by the electrostatic potential applied between the pipette and the collector. The most favourable value was usually in the range 1–3 kV/m, and could be found by a manual "trial and error" variation of the applied voltage. According to the simple model of the electro-bending instability proposed by Reneker et al [14], increased voltage increases the length of the rectilinear segment of the jet and decreases the angle of the spiral envelope. The model appears to appropriately describe the behavior of polyethylene-oxide solution (Fig. 4a).

For this solution, the bending instability treshold of the jet was observed at about 3 kV. Farther increase of the voltage elongates the straight part of the jet and leads to the development of relatively stable, large amplitude looping. The initial bending is nearly perpendicular to the jet direction. Above 5 kV the spiral envelope angle decreases while the length of the straight portion of the fibre increases further. It is worth noting that at slightly lower polymer concentration (3%) high amplitude oscillations of the straight segment length were observed. Similar oscillations were reported by Theron et al. [2] and interpreted as an effect of the competition between the supply of liquid and its withdrawal by the electric field. Future investigations are necessary to elucidate the nature of this unstable interaction.

Experiments performed for DBC solutions show an opposite relation for the location of the first bending (Fig. 3b), i.e. the length of the straight segment diminishes with the applied voltage. Only above 12 kV this trend reverses, but farther increase of the voltage quickly terminates the looping process. The third investigated polymer solution (PAN) exhibits more or less the same behaviour (comp. Fig. 4c) as with PEO.

There are several possible factors which could be responsible for the observed differences. Solidification of the polymer, not controlled in the experiment, is one of the factors which may totally modify the development of the bending instability. The mechanical properties of the looping fibre evolves continuously along its path in a manner that is difficult to predict, being influenced by local stresses due to the external electrostatic force, by interaction of charges within each segment of the fibre, by solidification and solvent evaporation. Their influence on the highly non-linear process responsible for the electro-bending instability is difficult to estimate using simple mechanical models.

The most important fluid parameter responsible for the spinning process of polymers is viscoelasticity. However, it is worth to note that electrospinning is also possible for Newtonian fluids, and long looping sequences of glycerol jet could be observed (Fig. 5). The glycerol jet forms a relatively long and well controllable spiral before it atomises into tiny droplets due to the capillary instability. However, the stretching factor for Newtonian fluid is relatively small and amounts to approximately ten. Viscosity appears to be a very important factor in this configuration. By decreasing or increasing the contents of water in glycerol electrospinning disappears and the relatively straight jet breaks up into many small droplets several centimetres downstream from the tip.

Surface tension could be assumed to play a role affecting jet instability. For the four investigated fluids the surface tension is very similar, about 50 mN/m. It can be decreased by adding surface active agents to the solution. A sequence of experimental runs performed with the 4% PEO solution and different concentration of surface active additive could not highlight any clear effect of surface tension on the jet geometry, suggesting its effect is weak. Even small amounts of surfactant can change viscoelasticity and this way influence the stability of the electrospinning thread. But apparently for the investigated case this effect was not sufficient to significantly alter the electrospun (electrospun thread) process.

4. Numerical model

It is very difficult to use experimental data for validating the correctness of physical models of electrospinning proposed in the literature [14,23,24]. It is due to the difficulties in estimating proper values of the basic parameters necessary for modelling, such as charge density, electric field geometry, mass and charge flow rate, variation of fluid parameters and initial conditions. Hence, results of simulations have to be matched to the observations rather by fine turning of the input parameters. To estimate at least qualitatively the effect of basic parameters implemented in the model proposed by Reneker et al. [14,24] we perform sequence of simulations varying few of the control parameters and analysing the shape of fibre tracks produced by the model.

According to the model the jet dynamics is governed by a set of three equations representing the Maxwellian model of stretching viscoelastic segment, mass and momentum conservation for the electrically charged jet segments:

$$\frac{\partial \sigma(s)}{\partial t} = G\frac{1}{\lambda(s)}\frac{\partial \lambda(s)}{\partial t} - \frac{G}{\mu}\sigma(s) \tag{1}$$

$$\frac{D}{Dt}\left[\lambda(s)\pi a^2(s)\right] = 0 \tag{2}$$

$$\begin{aligned}
\rho\lambda(s)\pi a^2(s)\frac{D\mathbf{V}}{Dt}(s) &= \lambda(s)\pi a^2(s)q^2\int_0^s \lambda(s^*)\pi a^2(s^*) \\
&\times C\left(\frac{\bar{a}(s,s^*)}{|\mathbf{r}(s)-\mathbf{r}(s^*)|}\right)\frac{\mathbf{r}(s)-\mathbf{r}(s^*)}{|\mathbf{r}(s)-\mathbf{r}(s^*)|^3}ds^* \\
&+ \lambda(s)\pi a^2(s)q\nabla\Phi \\
&+ \frac{\partial}{\partial s}\left[\pi a^2(s)\sigma(s)\mathbf{u}(s)\right] \\
&+ \frac{\partial}{\partial s}\left[\pi a(s)\alpha\mathbf{u}(s)\right]
\end{aligned} \tag{3}$$

where σ is the longitudinal stress inside the fibre, G – the Young modulus, μ – the viscosity, λ – the stretching parameter (relative elongation with respect to the initial state), and s is the "frozen jet" Lagrangian parameter, which stretches together with the fibre. Writing the curvilinear coordinate ξ, the stretching parameter λ can thus be defined as $d\xi/ds$. By convention, $\sigma > 0$ corresponds to a tensile force and $\sigma < 0$ to compression. $D/Dt = \partial/\partial t + \mathbf{V} \cdot \nabla$ denotes the convective derivative, ρ is the fluid mass density, a is the local radii of the fibre, $\mathbf{r}$ is the absolute coordinate vector, $\mathbf{V}$ is the velocity vector, q is the charge per unit of volume, Φ is the electric potential generated by electrodes, $\mathbf{u}$ is a unit vector directed along the fibre and α is the surface tension. C is a short-range cut off function for Coulomb interactions, and depends on the ratio of the fibre radius to the distance between charges (comp. Appendix). Since this cut off is only relevant for small distances ($s^* \to s$), the average fibre radius $\bar{a}(s, s^*)$ can be defined in a quite loose manner, as long as the following conditions are fulfilled:

$$\lim_{s^* \to s} \bar{a}(s, s^*) = a(s) \tag{4}$$

$$\bar{a}(s, s^*) = \bar{a}(s^*, s) \tag{5}$$

The second condition is rather motivated by physical than mathematical considerations: it ensures that the Coulomb force acting on s from s^* remains exactly the opposite of the force acting from s^* to s. Some obvious possible candidates for the definition of $\bar{a}(s^*, s)$ are the geometrical or the arithmetical means of $a(s)$ and $a(s^*)$. The cut off function is given by

$$C(x) = \frac{2}{\pi} \frac{1}{4x^2 + 1} \mathrm{E}(2\mathrm{j}x), \tag{6}$$

where E stands for the complete elliptic integral of the second kind, j – imaginary number.

In our computer simulation a set of electrostatic charges coupled by viscoelastic one-dimensional elements subjected to surface tension effects evolves within a static electric field. The computationally expensive integration of Poisson equation is avoided by considering the electric potential as a superposition of an imposed static potential field and of a transient field created by the charges distributed along the fibre. The electrostatic field is modelled by a sphere-plane capacitor configuration, where the spherical electrode represents the injector and the infinite plane electrode represents the collector. The fibre-induced field is in turn approximated by considering only short range electric interactions, typically between a particle and its closest 30 neighbours.

Hence, numerical discretization in space considers only short range electric interactions, typically between a particle and its closest 30 neighbours. The following scheme is applied to solve the system of governing equations:

$$\frac{d\sigma_{i,i+1}}{dt} = G \frac{(\mathbf{r}_{i+1} - \mathbf{r}_i)(\mathbf{V}_{i+1} - \mathbf{V}_i)}{(\mathbf{r}_{i+1} - \mathbf{r}_i)^2} - \frac{G}{\mu}\sigma_{i,i+1}$$

$$\frac{d}{dt}\left(\pi|\mathbf{r}_i - \mathbf{r}_{i+1}|a_{i,i+1}^2\right) = 0$$

$$m_i \frac{d\mathbf{V}_i}{dt} = Q^2 \sum_{j \neq i} C\left(\frac{\bar{a}_{i,j}}{|\mathbf{r}_i - \mathbf{r}_j|}\right) \frac{\mathbf{r}_i - \mathbf{r}_j}{|\mathbf{r}_i - \mathbf{r}_j|^3}$$
$$- Q\nabla\Phi$$
$$+ \pi a_{i,i+1}^2 \sigma_{i,i+1} \frac{\mathbf{r}_{i+1} - \mathbf{r}_i}{|\mathbf{r}_{i+1} - \mathbf{r}_i|} \tag{7}$$
$$- \pi a_{i-1,i}^2 \sigma_{i-1,i} \frac{\mathbf{r}_i - \mathbf{r}_{i-1}}{|\mathbf{r}_i - \mathbf{r}_{i-1}|}$$
$$+ \pi a_{i,i+1}\alpha \frac{\mathbf{r}_{i+1} - \mathbf{r}_i}{|\mathbf{r}_{i+1} - \mathbf{r}_i|} - \pi a_{i-1,i}\alpha \frac{\mathbf{r}_i - \mathbf{r}_{i-1}}{|\mathbf{r}_i - \mathbf{r}_{i-1}|}$$

Q denotes the electric charge carried by a single bead and the "average" radius $\bar{a}_{i,j}$ is defined as:

$$\bar{a}_{i,j} = \begin{cases} \frac{1}{2}\left(a_{i,j+1} + a_{j-1,j}\right) & \text{if} \quad i < j \\ \frac{1}{2}\left(a_{j,j+1} + a_{i-1,j}\right) & \text{if} \quad i > j \end{cases} \tag{8}$$

Single subscripts such as i and j refer to beads, while subscript pairs such as $i, i + 1$ refer to the viscoelastic elements lying between consecutive beads. To initiate the computation the constant velocity of the first particle (subscript 0) introduced through the tip is imposed until the distance between the tip and this particle equals the initial bead length:

$$\mathbf{V}_0 = -\frac{\dot{V}}{\pi a_0^2}\mathbf{z} \quad \text{for} \quad |\mathbf{r}_0 - \mathbf{r}_{\mathrm{tip}}| \leq l_0, \tag{9}$$

where the volume flow rate $\dot{V}$, the initial radius a_0 and the initial bead length l_0 are considered as input data. When the condition $|\mathbf{r}_0 - \mathbf{r}_{\mathrm{tip}}| > l_0$ is satisfied a new particle is added near the tip at a distance l_0 from the last particle, with a small random error on its position in the $(\mathbf{x}, \mathbf{y})$ plane:

$$\begin{aligned} x_0 &= x_{\mathrm{tip}} + \varepsilon\sin\varphi \\ y_0 &= y_{\mathrm{tip}} + \varepsilon\cos\varphi \end{aligned} \tag{10}$$

where φ is a random phase and ε is perturbation amplitude. This initial perturbation is necessary to allow the instability to develop, but it has otherwise no bearing on the magnitude of the instability. The value of ε can be thus arbitrarily small (in theory) and it is in practice only dictated by computer precision considerations.

Using the leapfrog numerical scheme the system of discrete equations is integrated in time and position for each node representing discrete form of the charged jet segment evaluated. For a typical time step of 10^{-7} sec a complete run for the jet penetrating 20 cm distance from the electrode to the ground collector can be simulated during 2–3 min on a standard PC. It permits to perform sensitivity analysis of the model by generating large number of tracks for various input data. A demo version of the code can be downloaded and executed in Linux OS [25].

Figure 6 illustrates bending instability calculated for the reference case, i.e. the surface tension $\alpha = 0.07$ N/m, the voltage $\Phi = 5$ kV applied at 20 cm distance between electrodes, the dynamic viscosity $\mu = 10$ Pa·s, the elastic modulus $G = 10^5$ Pa, and the jet unit charge $q = 200$ C/m^3. It can be observed that the initial perturbation almost immediately develops to large amplitude bending of the jet. The elongation rate measured

as relative change of the distance between nodes reaches factor 10^3 shortly after the bending process is initiated. Higher elongation values can be observed when the jet approaches the ground electrode. The 20 cm distance between the source electrode and the ground collectors is traversed by the jet tip in less then 5 ms.

Five examples of calculated jet tracks for physical parameters varied around the reference case are collected in Fig. 7.
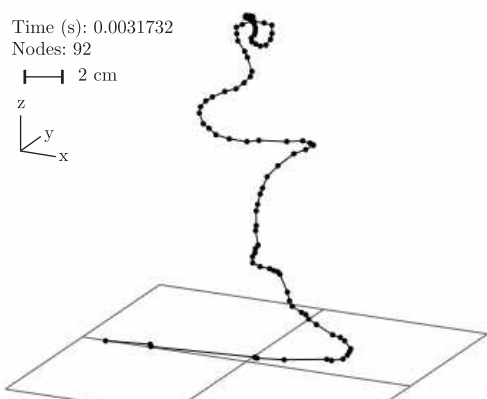

Fig. 6. Example of numerical simulations of electrostatic instability of charged liquid jet calculated for the reference parameters
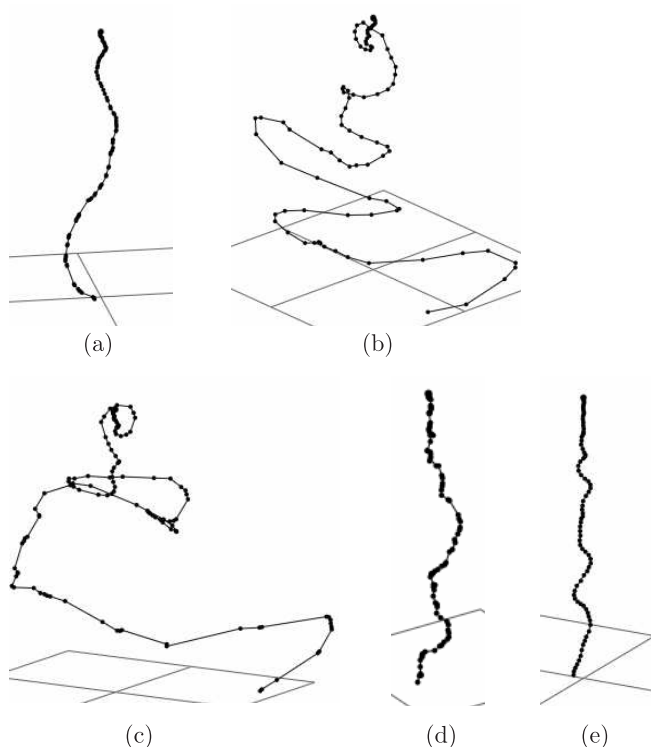

Fig. 7. Examples of numerical simulations of electrostatic instability of charged liquid jet obtained by changing the reference parameters: 3 times higher surface tension (a), 3 times lower surface tension (b), halved voltage (c), 5 times higher viscosity (d), double elastic modulus (e)

The model described above due to its simplicity is far from the realistic configuration. We assume fibre as an ideal insula-

tor of constant physical properties and induced charges moving in vacuum. To simplify our analysis we neglect very important for polymers effects of solidification. The fibre is represented as a chain of one dimensional dumbbells, hence capillary instability is absent. Despite these limitations some characteristics of the simulated fibre paths can be related to the observations. By comparing cases displayed in Figure 7a,b,e, it can be deduced that surface tension and elastic modulus stabilize jet and their increase ceases bending amplitude. By decreasing electrostatic potential (Fig. 7c), the bending amplitude grows. It partly corresponds to variation of the cone angle in the experiments (comp. Fig. 3a,b). Simulations indicate that increased fluid viscosity and elastic modulus limits the bending amplitude (Fig. 7d,e). The performed simulations show that some bending instability is still present even if elastic modulus is set to null. This zero-elasticity asymptotic behaviour appears to be analogous to Newtonian fluid (e.g. glycerol) jet.

5. Conclusions

Experimental investigation performed for three polymeric solutions and for glycerol demonstrated the possibility to stretch liquid jets in the electrical field into fractions of their initial diameter. Variety of jet paths are observed depending on the material and electrical potential applied. The present work repeats and corroborates previous observations [1,14,15], indicating appearance of the whipping instability for electrically charged liquid jets. Numerical simulations performed illustrate the ability of such a model to reproduce qualitatively nanofibre bending. However, it appears difficult to match quantitatively the observed electrospinning characteristics with the simulation results. In the farther perspective of using simulations as a design tool, outstanding modelling and numerical issues to be resolved include a better description of the boundary conditions at the tip and an efficient scheme to account for long range electric particle interactions. Quantitative validation of the electrostatic model can be eased by limiting our interest to Newtonian fluids, for example using aqueous solutions of glycerol. After such model is experimentally validated, the next step would be extension of the model to include rheology and solidification.

Appendix

A1. On the consistency of the discrete bead model

The discrete modelling of a fibre with 0-dimensional beads [14] implies that, as the discretization density increases, the fibre tends to an infinitely thin, one-dimensional continuous object. It turns out, however, that this continuous description is mathematically inconsistent, invalidating thus the discrete bead model. Indeed, the electrostatic force between two con-

tiguous portions of a straight fibre with constant radius and uniform charge distribution would amount to,

$$F_{1 \to 2} = \int_{-L_1}^{0} dz_1 \int_0^{L_2} dz_2 \frac{\kappa q_l^2}{(z_2 - z_1)^2} \qquad (A1)$$

where z_1 and z_2 are the locations of the interacting charges, L_1 and L_2 are the length of the two contiguous fibre portions, and q_l is the linear charge density of the fibre. It is easily seen that the double integral in Eq. (A1) is divergent.

This problem has been identified in the analytical study of Ref. [24] and resolved by arguing that charges are actually distributed on the outer shell of the fibre, rather than on its centre-line. Simplifications in the computations have lead, however, to an underestimation of the resulting cutoff which the present calculations hope to address. More generally, the following study aims at showing that the bead model can be made consistent by introducing a short-range cutoff.

A2. Force between two rings of a straight fibre

Let us consider a straight fibre of radius a charged on its outer shell with a uniform surface charge density q_s. Using the conventions of Fig. 8, the electrostatic force exerted by an infinitesimal surface element P_2 of the ring over S_2 an infinitesimal surface element P_1 of the ring S_1 in the coordinate system $(\mathbf{i}, \mathbf{j}, \mathbf{k})$ is

$$d\mathbf{F}_{P_2 \to P_1} = \kappa q_s^2 a d\theta_1 dz_1 a d\theta_2 dz_2$$
$$\times \frac{a(\cos\theta_1 - \cos\theta_2)\mathbf{i} + a(\sin\theta_1 - \sin\theta_2)\mathbf{j} + (z_1 - z_2)\mathbf{k}}{\{2a^2 [1 - \cos(\theta_2 - \theta_1)] + (z_2 - z_1)^2\}^{3/2}}.$$
$$(A2)$$

Computing the electrostatic force between two infinitely thin rings S_1 and S_2, the radial forces cancel to leave a longitudinal force along $\mathbf{k}$ equal to

$$dF_{S_2 \to S_1} = \kappa \frac{dQ_1 dQ_2}{4\pi^2} \int_0^{2\pi} d\theta_2 \int_0^{2\pi} d\theta_1$$
$$\times \frac{(z_1 - z_2)}{\{2a^2 [1 - \cos(\theta_2 - \theta_1)] + (z_2 - z_1)^2\}^{3/2}}.$$
$$(A3)$$

where $dQ_1 = 2\pi a q_s dz_1$ and $dQ_2 = 2\pi a q_s dz_2$ are the electrostatic charges of each ring. Introducing $\psi = (\theta_2 - \theta_1)/2$ and the distance between the center of the rings $d = |z_2 - z_1|$, the above expression can be simplified as follows:

$$dF_{S_2 \to S_1} = -\kappa \frac{dQ_1 dQ_2}{d^2} \times \frac{2}{\pi} \int_0^{\pi/2} \frac{d\psi}{\left[1 + (\frac{2a}{d})^2 \sin^2\psi\right]^{3/2}},$$
$$(A4)$$

where the second factor represents the short-range cutoff. This cutoff function can in turn be expressed in term of the complete elliptic integral of the second kind E as,

$$C(\hat{d}) = \frac{2}{\pi} \frac{1}{1 + (\frac{2}{\hat{d}})^2} \mathrm{E}\left(\frac{2j}{\hat{d}}\right)$$
$$= \frac{1}{\pi} \frac{\hat{d}}{\pi\sqrt{1 + \frac{1}{4}\hat{d}^2}} \mathrm{E}\left(\frac{1}{\sqrt{1 + \frac{1}{4}\hat{d}^2}}\right) \text{ with } \hat{d} = \frac{d}{a}.$$
$$(A5)$$

We note that the cutoff function presents the following asymptotic behaviours,

$$C(\hat{d}) \overset{\hat{d} \to 0}{\propto} \frac{\hat{d}}{\pi}$$
$$\lim_{\hat{d} \to \infty} C(\hat{d}) = 1 \qquad (A6)$$

The axial force between two rings behaves thus as d^{-1} as the distance between them vanishes. For comparison, the short-range axial force behaves as d in the simplified approach of Ref. [24]. This difference is due to the fact that instead of considering the interaction between two rings, Ref. [24] considers the interaction between a ring and a point located on the axis of the fibre.
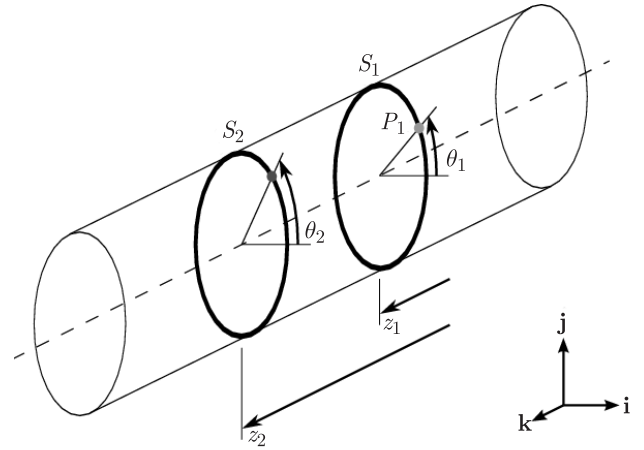

Fig. 8. Charges on two interacting rings of a straight fibre

A3. Axial and bending force between two rings of a curved fibre

Let us now consider a curved fibre. Using the conventions of Fig. 9, the electrostatic force exerted by an infinitesimal surface element P_2 of the ring S_2 over an infinitesimal surface element P_1 of the ring S_1 in the local coordinate system $(\mathbf{i}_1, \mathbf{j}_1, \mathbf{k}_1)$ of S_1 is

$$d\mathbf{F}_{P_2 \to P_1} = \kappa q_s^2 a d\theta_1 R d\alpha_1 a d\theta_2 R d\alpha_2$$
$$\times \frac{(x_1 - x_2)\mathbf{i}_1 + (y_1 - y_2)\mathbf{j}_1 + (z_1 - z_2)\mathbf{k}_1}{[(x_1 - x_2)^2 + (y_1 - y_2)^2 + (z_1 - z_2)^2]^{3/2}}$$
$$(A7)$$

where

$$x_1 - x_2 = a(\cos\theta_1 - \cos\theta_2) \qquad (A8)$$
$$y_1 - y_2 = a(\sin\theta_1 - \sin\theta_2) - (R - a\sin\theta_2)[1 - \cos(\alpha_2 - \alpha_1)]$$
$$(A9)$$
$$z_1 - z_2 = -(R - a\sin\theta_2)\sin(\alpha_2 - \alpha_1) \qquad (A10)$$

Assuming that the radius of curvature is large with regard to the radius of the fibre,

$$R \gg a \qquad (A11)$$

and noting that the distance between the centres of the rings is

$$d = 2R \left|\sin\left(\frac{\alpha_2 - \alpha_1}{2}\right)\right|, \qquad (A13)$$

the expression of the force simplifies to

$$dF_{P_2 \to P_1} = \kappa q_s^2 a\,d\theta_1 R\,d\alpha_1 a\,d\theta_2 R\,d\alpha_2$$

$$\times \left\{ \frac{a(\cos\theta_1 - \cos\theta_2)\mathbf{i}_1}{\left\{2a^2\left[1 - \cos(\theta_2 - \theta_1)\right] + d^2\right\}^{3/2}} \right.$$

$$+ \frac{\left\{a(\sin\theta_1 - \sin\theta_2) - R + R\cos(\alpha_2 - \alpha_1)\right\}\mathbf{j}_1}{\left\{2a^2\left[1 - \cos(\theta_2 - \theta_1)\right] + d^2\right\}^{3/2}}$$

$$+ \left. \frac{R\sin(\alpha_2 - \alpha_1)\mathbf{k}_1}{\left\{2a^2\left[1 - \cos(\theta_2 - \theta_1)\right] + d^2\right\}^{3/2}} \right\}$$
$$(A14)$$

Just as in the case of a straight fibre, the terms in θ in the nominator will eventually cancel when integrating over θ_1 and θ_2, so that they may be eliminated a priori in the expression of the force exerted by the ring S_2 over the ring S_1,

$$dF_{S_2 \to S_1} = \kappa \frac{dQ_1 dQ_2}{4\pi^2} \int_0^{2\pi} d\theta_1 \int_0^{2\pi} d\theta_2$$

$$\times \frac{R[\cos(\alpha_2 - \alpha_1) - 1]\mathbf{j}_1 - R\sin(\alpha_2 - \alpha_1)\mathbf{k}_1}{\left\{2a^2\left[1 - \cos(\theta_2 - \theta_1)\right] + d^2\right\}^{3/2}}.$$
$$(A15)$$

The nominator is constant with respect to θ_1 and θ_2 while the denominator is formally identical to the one obtained in the case of a straight fibre. Therefore, the same cutoff function C as before appears after integration,

$$dF_{S_2 \to S_1} = \kappa \frac{dQ_1 dQ_2}{d^3} C\left(\frac{d}{a}\right) R$$

$$\times \left\{[\cos(\alpha_2 - \alpha_1) - 1]\mathbf{j}_1 - \sin(\alpha_2 - \alpha_1)\mathbf{k}_1\right\}.$$
$$(A16)$$

It is easily verified that this expression differs from the case of an infinitely thin fibre only by the factor $C(d/a)$. Therefore, the discretised bead model can be made consistent by simply weighting the computed force with the cutoff function.
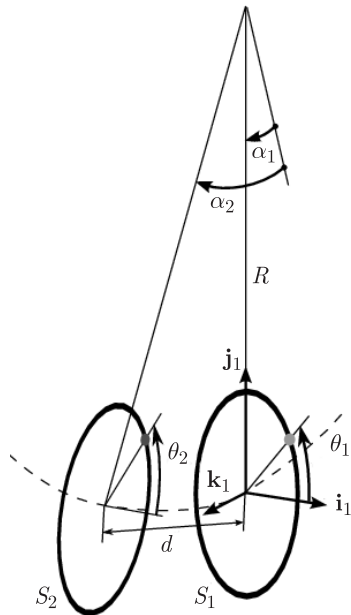

Fig. 9. Charges on two interacting rings of a curved fibre

Using Eq. (A13) it can be noted that for small distances the projection of dF on $\mathbf{j}_1$ (bending component) tends to a finite, non-zero value, to be contrasted with the d^2 behavior found previously [24]. As could be expected from the hypothesis $R \gg a$, the projection of dF on $\mathbf{k}_1$ (axial component) behaves just like in the case of a straight fibre, i.e. in d^{-1}.

REFERENCES

[1] A.L. Yarin, "Electrospinning of nanofibers from polymer solutions and melts", *Lecture Notes* 5, IPPT PAN and CoE AMAS, Warsaw, 2003.

[2] S.A. Therona E. Zussman, and A.L. Yarin, "Experimental investigation of the governing parameters in the electrospinning of polymer solutions", *Polymer* 45, 2017–2030 (2004).

[3] P. Gibson and H. Schreuder-Gibson, "Patterned electrospun polymer fiber structures", *e-Polymers* 002, 1–15 (2003).

[4] Z. Jun, H. Hou, A. Schaper, J.H. Wendorff, and A. Greiner, "Poly-L-lactide nanofibers by electrospinng – Influence of solution viscosity and electrical conductivity on fiber diameter and fiber morphology", *e-Polymers* 009, 1–9 (2003).

[5] P. Gibson, H. Schreuder-Gibson, and D. Riven, "Electrospun fiber mats: transport properties", *AIChE J* 45, 190–195 (1999).

[6] H.J. Jin, A. Fridrikh, G.C. Rutledge, and D. Kaplan, "Electrospinning Bombyx mori silk with poly(ethylene oxide)", *Abstr. Pap. Am. Chem. Soc.* 224, 408 (2002).

[7] A.C. MacDiarmid, W.E. Jones, I.D. Norris, J. Gao, A.T. Johnson, N.J. Pinto, J. Hone, B. Han, F.K. Ko, H. Okuzaki, and M. Llanguno, "Electrostatically generated nanofibers of electronic polymers", *J. Synth. Metals* 119, 27–30 (2001).

[8] I.D. Norris, M.M. Shaker, F.K. Ko, and A.G. MacDiarmid, "Electrostatic fabrication of ultrafine conducting fibers: polyaniline/polyethylene oxide blends", *J Synth. Metals* 114, 109–14 (2000).

[9] T.A. Kowalewski, "On separation of droplets from a liquid jet", *Fluid Dyn. Res.* 17, 121–145 (1996).

[10] A.L. Yarin, *Free Liquid Jest and Films: Hydrodynamics and Rheology*, Longman Scientific & Technical, New York, 1993.

[11] A. Ziabicki and H. Kawai, *High- speed Fiber Spinning: Science and Engineering Aspects*, John Wiley & Sons, Inc, New York, 1985.

[12] Lord Rayleigh (J.W. Strutt), "On the equilibrium of liquid conducting masses charged with electricity", *Philos. Mag.* 44, 184–186 (1882).

[13] G.I Taylor, "Disintegration of water drops in an electric field", *Proc. R. Soc. London* A 280, 383–397 (1964).

[14] D.H. Reneker, A.L. Yarin, H. Fong, and S. Koombhongse, "Bending instability of electrically charged liquid jets of polymer solutions in electrospinning", *J. Appl. Phys.* 87, 4531–4547 (2000).

[15] M. Shin, M.M. Hohman, M.P. Brenner, and G.C. Rutledge, "Electrospinning: A whipping fluid jet generates submicron polymer fibers", *Appl. Phys. Lett.* 78, 1149 – 1151 (2001).

[16] A. Formhals, "Process and apparatus for preparing of artificial threads", U.S. Pat. 1,975,504 (1934).

[17] M.M. Hohman, M. Shin, G. Rutledge, and M.P. Brenner, "Electrospinning and electrically forced jets I: stability theory", *Phys. Fluids* 13, 2201–2220 (2001).

[18] M.M. Hohman, M. Shin, G. Rutledge, and M.P. Brenner, "Electrospinning and electrically forced jets II: applications", *Phys. Fluids* 13, 2221–2236 (2001).

[19] A.L. Yarin and E. Zussman , "Upward needleless electrospinning of multiple nanofibers", *Polymer* 45, 2977–2980 (2004).

[20] J. Doshi and D. H. Reneker, "Electrospinning process and applications of electrospun fibers", *J. Electrost.* 35, 151-160 (1995).

[21] B. Tchavdarov, A.L. Yarin, and S. Radev, "Buckling of thin liquid jets", *J. Fluid Mech.* 253, 593–615 (1993).

[22] A. Theron, E. Zussman, and A.L. Yarin, "Electrostatic field-assisted alignment of electrospun nanofibers", *Nanotechnology* 12, 384–390 (2001).

[23] J.J. Feng, "The stretching of an electrified non-Newtonian jet: A model for electrospinning", *Physics of Fluids* 14, 3912–26 (2002).

[24] A.L. Yarin, S. Koombhongse, and D.H. Reneker, "Bending instability in electrospinning of nanofibers", *J. Appl. Phys.* 89, 3018–3026 (2001).

[25] S. Barral, "Fibre 3D – program simulating electrospinning" (2005), `http://fluid.ippt.gov.pl/nanofibres/fibre3d`.